ACS APPLIED MATERIALS & INTERFACES

Research Article

www.acsami.org

Double-Shelled CdS- and CdSe-Cosensitized ZnO Porous Nanotube Arrays for Superior Photoelectrocatalytic Applications

Pan-Yong Kuang,[†] Yu-Zhi Su,[†] Kang Xiao,[†] Zhao-Qing Liu,*[,†] Nan Li,[†] Hong-Juan Wang,[†] and Jun Zhang*[,‡]

[†]School of Chemistry and Chemical Engineering/Guangzhou Key Laboratory for Environmentally Functional Materials and Technology, Guangzhou University, Guangzhou 510006, PR China

[‡]State Key Laboratory of Advanced Technology for Materials Synthesis and Processing, Wuhan University of Technology, Wuhan 430070, PR China

Supporting Information

ABSTRACT: The effective separation and transport of photoinduced electron−hole pairs in photoanodes is of great significance to photoelectrochemical and catalytic performance. Here, a facile and effective two-step strategy is developed to fabricate double-shelled ZnO/CdS/CdSe porous nanotube photoanodes from ZnO nanorod arrays (NRAs). Surprisingly, after the process of the deposition of CdS and CdSe, the ZnO nanorod arrays are partially dissolved, resulting in the formation of ZnO/CdS/CdSe porous nanotube arrays (NTAs). By virtue of their unique porous nanotube structure and cosensitization effect, the ZnO/CdS/CdSe porous NTAs show superior photoelectrochemical water-splitting performance and organic-pollutant-degradation ability under visible light irradiation, as well as excellent long-term photostability.

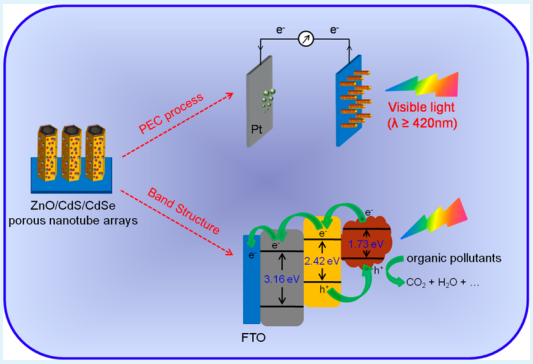

KEYWORDS: *double-shelled, ZnO/CdS/CdSe, porous nanotube, cosensitization effect, organic pollutants degradation*

INTRODUCTION

Solar-energy-driven photoelectrochemical water-splitting has been considered as an ideal route to cope with the global energy crisis and environmental problems due to its endless supply of light and water resources. Research on water-splitting has gained increasing attention since Fujishima and Honda first reported the electrochemical photolysis of H_2O on a TiO_2 photoanode.[1] To date, numerous metal oxide semiconductors such as ZnO, TiO_2, and Fe_2O_3 have drawn more and more attention in photoelectrochemistry.[2−4] Among them, ZnO has been extensively investigated for energy conversion devices[5−7] due to its high carrier mobility,[8] ease of synthesis,[9] and nontoxicity.[10] However, several unfavorable drawbacks, such as a wide band gap (E_g = 3.2 eV) and fast internal recombination of charge carriers, lead to low quantum yields and poor solar conversion efficiency.[11,12] In this regard, it is highly desirable to improve the photocatalytic efficiency of ZnO under visible light irradiation.

In recent years, the chalcogenide compounds CdS,[13,14] CdSe,[15,16] and CdTe[17,18] have been intensively employed as sensitizers of wide band gap semiconductors such as ZnO and TiO_2 photoanodes. Generally, the staggered band gap structure of the photoanode and sensitizers always follow the typical type-II mode, where both the valence and the conduction bands of the sensitizers are higher in energy than those of the photoanodes,[19,20] which causes the spatial separation and facilitates the charge transfer, thus reducing the internal charge recombination and promoting the photocatalytic activity.[21] Consequently, due to the narrow band gaps ($E_{g,CdS}$ = 2.4 eV; $E_{g,CdSe}$ = 1.7 eV) and suitable band gap structures,[22] these chalcogenide compound modifications could significantly improve the visible light absorption and energy conversion efficiency in quantum-dot-sensitized solar cells (QDSSCs) and photoelectrochemical and photovoltaic devices.[23] Moreover, the CdS/CdSe-cosensitized system exhibits further enhanced performance to those sensitized only by CdS or CdSe because of the combination of advantages of the two sensitizers and the stepwise band-edge structure.[24] For example, Wang[25] fabricated a double-sized cosensitized photoanode system that obtains a photocurrent density of 12 mA cm^{-2} at 0.4 V versus Ag/AgCl in photoelectrochemical hydrogen generation. The power conversion efficiency of 1.42% was achieved for CdS/CdSe-cosensitized ZnO solar cells under the full spectrum illumination.[26] Inspiringly, Seol[27] have assembled CdS and CdSe onto the surface of ZnO nanowire arrays and obtained a power conversion efficiency of 4.15%. Moreover, a high power efficiency of 4.22% and a saturated photocurrent of 14.9 mA cm^{-2} have been achieved in the TiO_2/CdS/CdSe solar cells.[28] Despite the fact that most researchers are focused on CdS- and CdSe-cosensitized ZnO and TiO_2 nanorods or nanowires, there

Received: April 23, 2015
Accepted: July 14, 2015
Published: July 14, 2015

DOI: 10.1021/acsami.5b03527
ACS Appl. Mater. Interfaces 2015, 7, 16387−16394

Scheme 1. Fabrication Process of the ZnO/CdS/CdSe Porous NTAs

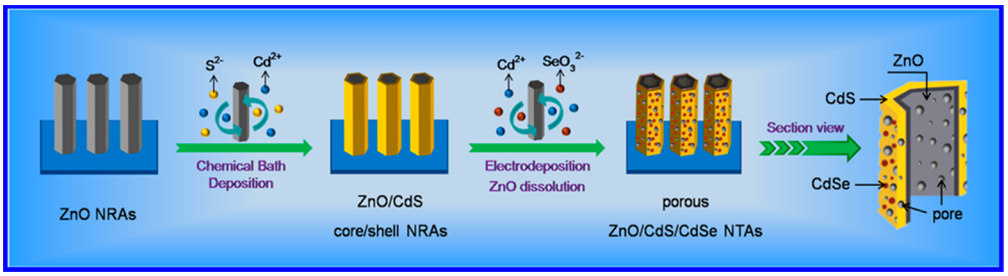

are few reports on the preparation of a ZnO/CdS/CdSe porous nanotube structure and its visible-light photoelectrochemical performance. Indeed, the porous nanotubes have stimulated much interest due to their larger surface area[29] and more efficient charge carrier extraction.[30]

In this work, we develop a facile and effective strategy to fabricate the double-shelled ZnO/CdS/CdSe porous nanotube arrays (NTAs) from ZnO nanorod arrays (NRAs). The ZnO/CdS/CdSe porous NTAs are composed of a CdS shell, CdSe nanoparticles, and a thin, porous ZnO nanotube structure, which could facilitate the mass transfer of reactants, provide a large contact area, and expose more catalytic sites (especially those located in the inner wall of ZnO/CdS/CdSe nanotube and pores). Compared to the single-shelled ZnO/CdS and ZnO/CdSe structures, the synergetic effect of CdS and CdSe could be beneficial to the visible-light absorption and charge separation abilities of ZnO/CdS/CdSe porous NTAs, resulting in high photoelectrochemical performances.

EXPERIMENTAL SECTION

Chemicals and Materials. $Zn(NO_3)_2{\cdot}6H_2O$, NH_4Ac, $C_6H_{12}N_4$ (HMT), $Cd(NO_3)_2{\cdot}4H_2O$, thiourea (CN_2H_4S), $Cd(Ac)_2{\cdot}2H_2O$, ethylenediamine tetraacetic acid disodium salt (EDTA−2Na), Na_2SeO_3, and methylene blue (MB) were purchased from Sinopharm Chemical Reagent Co., Ltd. (Shanghai, China) and were used directly without further treatment.

Synthesis of ZnO NRAs. According to the previous report,[31] ZnO NRAs were grown on fluorine tin oxide (FTO) substrate through electrodeposition with a current density of −2.0 mA cm^{-2} and a depositon time of 50 min. A mixed aqueous solution containing 0.02 M $Zn(NO_3)_2$, 0.01 M NH_4Ac, and 0.01 M HMT served as the electrolyte, and the reaction temperature was kept at 90 °C. In the process of cathodic electrodepositon, a FTO substrate with a sheet resistance of 14 Ω/□, and a graphite rod was used as the working electrode and counter electrode, respectively. Finally, the FTO substrate covered with ZnO NRAs was washed thoroughly with distilled water and then dried at room temperature.

Fabrication of ZnO/CdS/CdSe Porous NTAs. The ZnO/CdS/CdSe porous NTAs were synthesized via the two-step chemical bath deposition (CBD) and electrodeposition processes. An aqueous solution composed of 0.01 M $Cd(NO_3)_2$ and 0.01 M thiourea, listed as solution A, served as the electrolyte in the CBD for CdS shell. The FTO substrate covered with ZnO NRAs was immersed into the above solution A for 30 min, and the reaction temperature was kept at 90 °C. Subsequently, an aqueous solution composed of 0.02 M $Cd(Ac)_2$, 0.02 M Na_2SeO_3, and 0.04 M EDTA−2Na, listed as solution B, worked as the electrolyte for the electrodeposition of CdSe; the FTO substrate covered with ZnO/CdS nanorods and a platinum sheet served as the working electrode and the counter electrode, respectively. The current density was −1.5 mA cm^{-2}, and the deposition time was 15 min. Similarly, the ZnO/CdS and ZnO/CdSe NRAs can be obtained through CBD and electrodeposition, respectively. The fabrication process of ZnO/CdS/CdSe porous NTAs was presented in Scheme 1.

Characterizations. Powder X-ray diffraction (XRD) measurement was conducted on a PANalytical PW3040/60 diffractometer with monochromatized Cu Kα radiation (λ = 0.15418 nm). The surface morphology and crystal microstructure of samples were examined using field emission scanning electron microscopy (FE-SEM, JEOL JSM-7001F) equipped with an energy-dispersive spectroscopy (EDS) device as well as transmission electron microscopy (TEM, JEM2010-HR). The surface electronic states and the compositions of the sample were analyzed by X-ray photoelectron spectroscopy (XPS, ESCALab250). The UV−vis diffuse reflectance spectra (UV−vis DRS) of samples were obtained over a UV−vis spectrophotometer (Cary 300) using $BaSO_4$ as the reference.

Photoelectrochemical Measurements. Conventionally, a single-compartment quartz cell with three electrodes, equipped with a CHI 760D model electrochemical workstation (Shanghai Chenhua), was used for photoelectrochemical measurements, where the as-prepared photoanode was used as the working electrode (the available electrode area immersed in the solution was fixed to 2.25 cm^2), and the saturated calomel electrode (SCE) and platinum sheet (1 cm × 1 cm) served as the reference and counter electrode, respectively. In the photoelectrochemical experiments, a 0.25 M Na_2S and 0.35 M Na_2SO_3 aqueous solution served as the electrolyte, and a regulable 300 W Xe lamp with an ultraviolet filter (λ > 420 nm) was used as the light source; the distance positioned to the quartz cell was about 10 cm, and the light intensity of light source is about 100 mW/cm^2.

The photoelectrocatalytic activities of the as-prepared photoanodes were evaluated by degrading methylene blue (MB) solution. In a typical process, 5 mL of 20 mg L^{-1} MB solution was added into 50 mL of 0.1 M Na_2SO_4 solution to form a homogeneous aqueous solution. Prior to irradiation, the as-prepared electrode was immersed into the solution and then magnetically stirred for 30 min in the dark to establish an adsorption−desorption equilibrium of dyes on the catalysts. Afterward, a 300 W Xe lamp with a 420 nm cutoff filter was introduced to the system, and a bias voltage of 0.5 V was employed to impel the photoinduced electron transfer from the working electrode to the counter electrode. At regular time intervals, about 3 mL of the solution was collected and analyzed with a UV−vis absorption spectrometer to determine the conversion rate of MB solution.

DOI: 10.1021/acsami.5b03527
ACS Appl. Mater. Interfaces 2015, 7, 16387−16394

RESULTS AND DISCUSSION

Figure 1 shows the typical XRD patterns of the as-prepared photoanodes. For the pristine ZnO NRAs, the strong

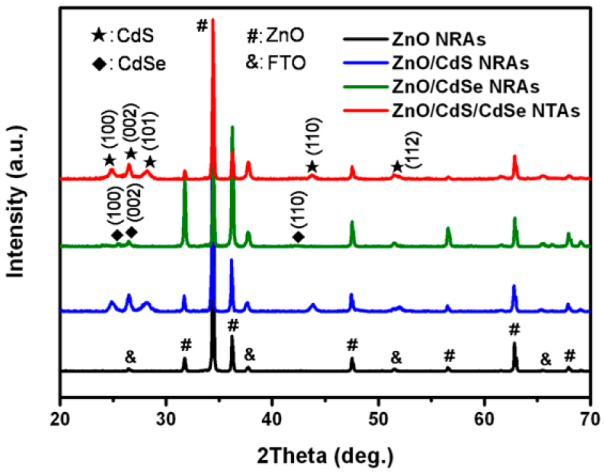

Figure 1. XRD patterns of ZnO, ZnO/CdS, ZnO/CdSe, and ZnO/CdS/CdSe.

diffraction peaks can be indexed to the hexagonal wurtzite phase of ZnO (JCPDS: 36−1451, $a = b = 3.25$ Å, $c = 5.21$ Å). Meanwhile, apparent peaks of CdS and CdSe are observed after the deposition process, which can be well-indexed to the hexagonal phase of CdS (JCPDS: 41−1049, $a = b = 4.14$ Å, $c = 6.72$ Å) and hexagonal phase of CdSe (JCPDS: 65−3436, $a = b = 4.30$ Å, $c = 7.01$ Å), respectively. Furthermore, no traces of other peaks can be observed, confirming that ZnO, CdS, and CdSe with high purity were obtained.

The scanning electron microscopy (SEM) and transmission electron microscopy (TEM) images depict the morphology and microstructure of the as-prepared photoanodes. Figure S2 in the Supporting Information shows the top and enlarged view of the preformed ZnO NRAs, which are hexagonally and uniformly distributed on the FTO substrate with a diameter of ca. 250−300 nm. The panoramic and magnified images after the deposition of CdS and CdSe shells are displayed in Figure 2a,b; the hexagonal nanorod structures remained with almost no change compared to the pure ZnO nanorod, and the average diameter increases obviously. Surprisingly, the shells are composed of numerous nanoparticles, and many pores are formed between these nanoparticles. The corresponding TEM images (Figure 2c,d) further confirm the construction of core and shell porous nanotube structure for ZnO/CdS/CdSe. The formation of such a porous nanotube hollow structure can be mainly attributed to the partial dissolution of ZnO in the central region during the deposition process of CdS and CdSe (as shown in Scheme 1). Figure 2e exhibits the high-resolution transmission electron microscope (HRTEM) image of the ZnO core and CdS and CdSe shell; the lattice spacing of 0.260 nm corresponds to the (002) plane of ZnO in the wurtzite phase, and the lattice fringe spacing of 0.152 nm matches well with the interplanar distances of the (104) plane of hexagonal CdS. Meanwhile, the lattice fringe spacings of 0.255 and 0.372 nm agree well with the interplanar distances of the (102) and (100) planes of hexagonal CdSe, respectively. Furthermore, the interface is very compact and continuous, which could favor the vectorial transfer of charge carriers among the components of the photoanode. Additionally, there are only O, Zn, S, Se, and Cd elements in the EDX spectrum (Figure 2f), which further demonstrates the high purity of ZnO, CdS, and CdSe. Moreover, the intensities of O, Zn, and Se elements are quite weak compared to the S and Cd elements, from which we can deduce that ZnO was dissolved mostly after the deposition process of CdS and CdSe. On the other hand, the weak intensity of Se indicates the small quantity and random distribution of CdSe on the CdS layer, which is also consistent with the TEM image in Figure 2d. From the above discussion, it can be inferred that the ZnO/CdS/CdSe porous NTAs have been successfully synthesized. The morphology and microstructure of ZnO/CdS and ZnO/CdSe NRAs are also presented in Figures S3 and S4 in the Supporting Information.

The surface electronic states and composition of the ZnO/CdS/CdSe porous NTAs were analyzed by X-ray photoelectron spectroscopy. Figure 3a shows the typical XPS survey spectra; the presence of only Zn, Cd, O, S, and Se elements further demonstrates the high purity of the products. The two symmetric peaks at binding energies of 1021.5 and 1044.6 eV

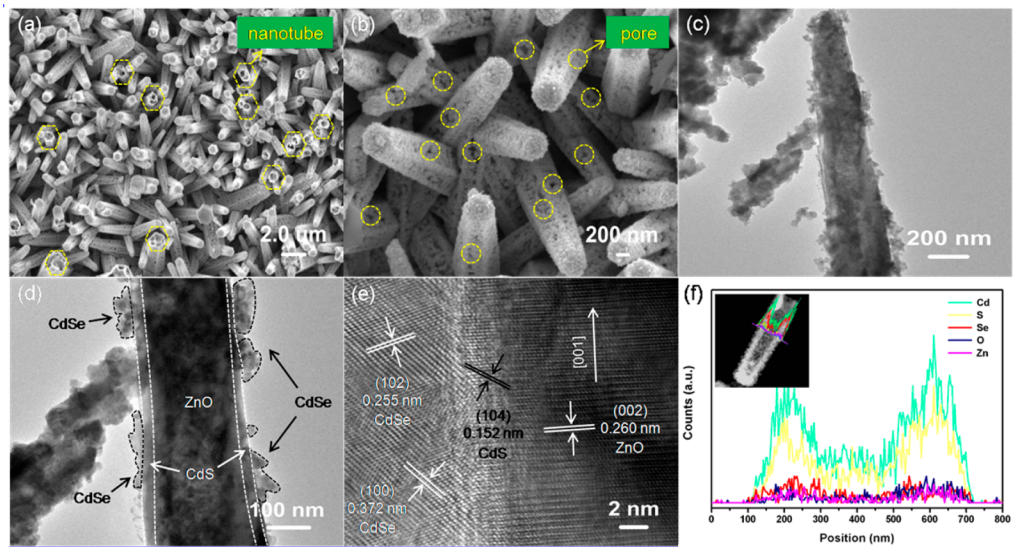

Figure 2. (a,b) SEM images, (c,d) TEM images, (e) a high-resolution TEM image, and (f) the EDX spectrum of ZnO/CdS/CdSe porous NTAs.

DOI: 10.1021/acsami.5b03527
ACS Appl. Mater. Interfaces 2015, 7, 16387−16394

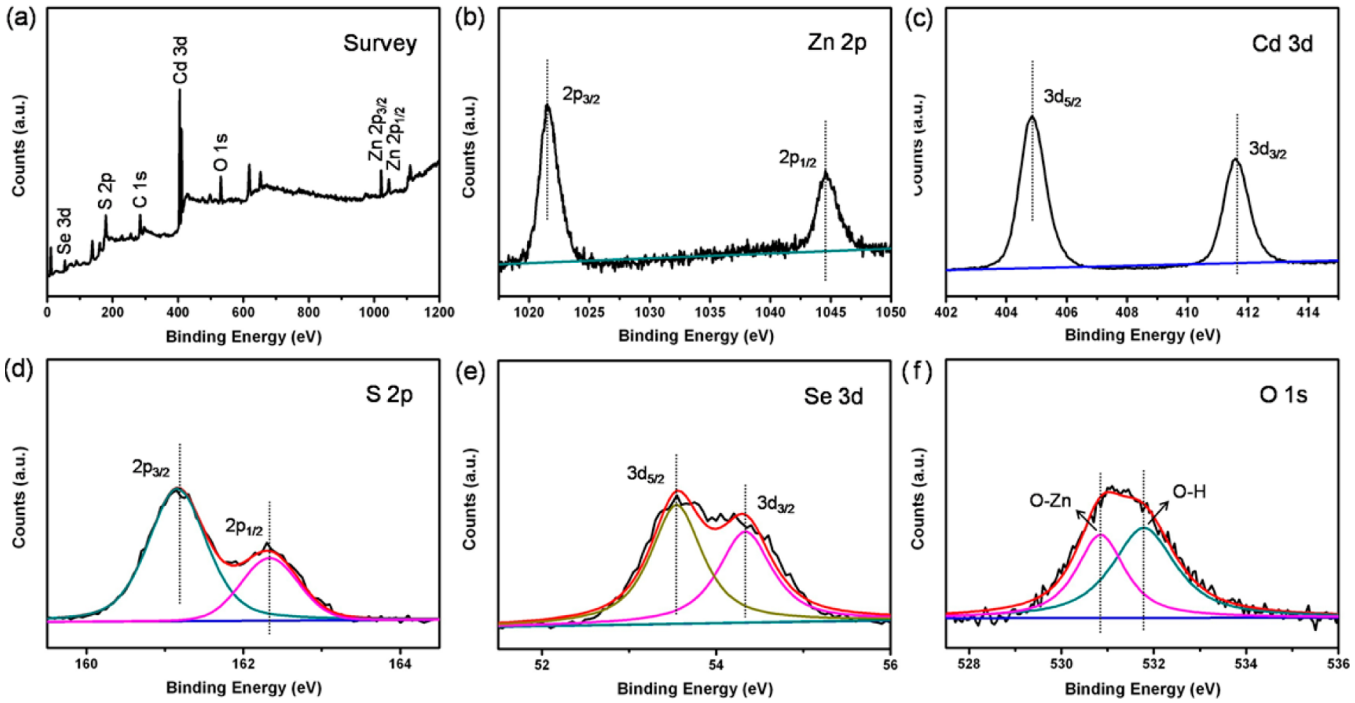

Figure 3. XPS spectra of ZnO/CdS/CdSe: (a) survey, (b) Zn 2p, (c) Cd 3d, (d) S 2p, (e) Se 3d, and (f) O 1s.

in the high-resolution spectrum are assigned to Zn $2p_{3/2}$ and Zn $2p_{1/2}$ (Figure 3b), which is in agreement with the previous report for ZnO.[32,33] The high-resolution spectrum of Cd 3d in Figure 3c with featured peaks of $3d_{5/2}$ at 404.9 eV and $3d_{3/2}$ at 411.6 eV indicates the +2 oxidation state (Cd^{2+}) in the as-prepared ZnO/CdS/CdSe.[34] Figure 3d exhibits the high-resolution spectrum of S 2p extracted from the ZnO/CdS/CdSe; the two peaks located at 161.2 and 162.3 eV are associated with S $2p_{3/2}$ and S $2p_{1/2}$, which are ascribed to the hybrid chemical bond species of S^{2-} and Cd−S.[35] Meanwhile, the two peaks located at 53.6 and 54.3 eV in Figure 3e are mainly attributed to Se $3d_{5/2}$ and Se $3d_{3/2}$, respectively, revealing the value state of Se^{2-} in ZnO/CdS/CdSe.[36] As presented in Figure 3f, the O 1s peak can be deconvoluted into two peaks at around 530.9 and 531.8 eV, corresponding to the Zn−O bonds of ZnO[37] and the adsorbed O_2 or surface hydroxyl species,[38] respectively. In addition, the XPS spectra of ZnO/CdS and ZnO/CdSe NRAs in Figure S5 in the Supporting Information are also consistent with the discussion of ZnO/CdS/CdSe NTAs. The above XRD and XPS results demonstrate the coexistence of ZnO, CdS, and CdSe in the as-prepared photoanodes.

UV−vis diffuse reflectance spectra were measured to investigate the optical properties of samples. As presented in Figure 4a, the pristine ZnO exhibits almost no absorption in the visible light region due to its wide band gap (ca. 3.2 eV). While the absorption intensity of ZnO/CdS, ZnO/CdSe, and ZnO/CdS/CdSe increase apparently in the visible-light range, red shifts (in comparison to ZnO) occurred. After decoration by a single CdS and CdSe shell, absorption edges of about 560 and 680 nm were observed, which are consistent with the band gap of the bulk counterparts ($E_{g,CdS} \approx 2.4$ eV and $E_{g,CdSe} \approx 1.7$ eV, respectively). The red shift of ZnO/CdSe is larger than that of ZnO/CdS due to the lower band gap of CdSe. It is worth noting that the ZnO/CdS/CdSe porous NTAs further extend the absorption range and increase their absorbance compared

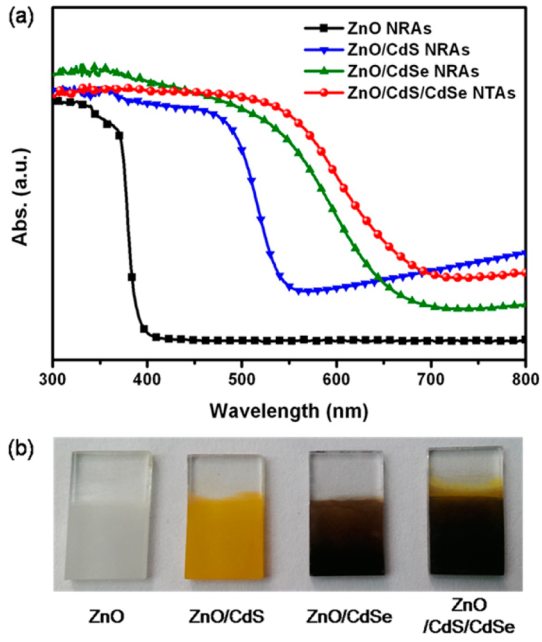

Figure 4. (a) UV−vis diffuse reflectance spectra and (b) corresponding colors of bare ZnO, ZnO/CdS, ZnO/CdSe, ZnO/CdS/CdSe, and ZnO/CdSe/CdS.

with the qualities of the single-shelled photoanodes. The enhanced visible light absorption of ZnO/CdS/CdSe porous NTAs may be attributed to the presence of both visible-light responsive CdS and CdSe, which induced the cosensitization effect.[39]

To evaluate the photoelectrochemical performance of the as-prepared single and double-shelled photoanodes, we conducted photoelectrochemical measurements in 0.25 M Na_2S and 0.35 M Na_2SO_3 solution. Figure 5a shows the current density-potential ($J-V$) characteristics of the photoanodes under

DOI: 10.1021/acsami.5b03527
ACS Appl. Mater. Interfaces 2015, 7, 16387−16394

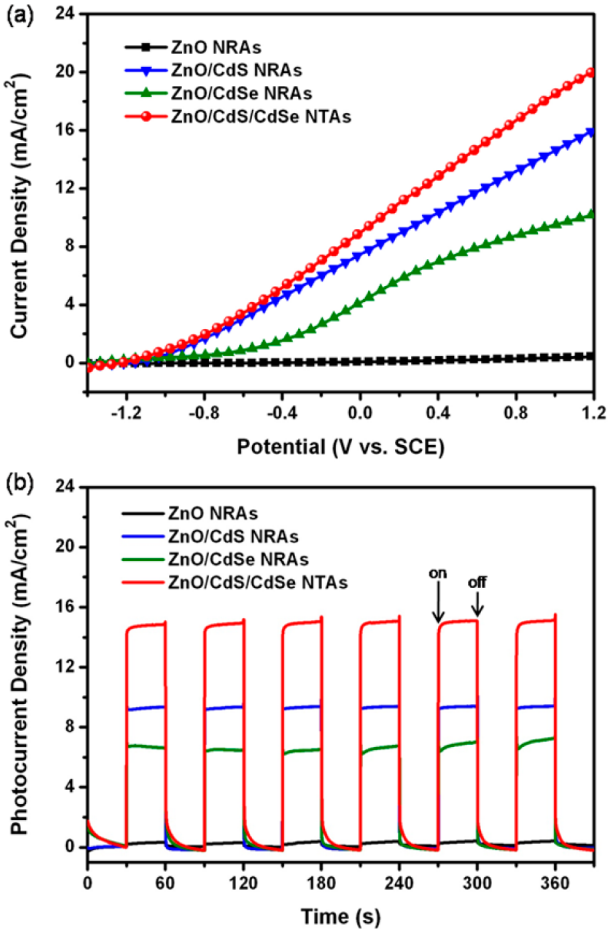

Figure 5. (a) Current density versus the applied potential characteristics (10 mV/s) and (b) photocurrent response to light on−off of the ZnO, ZnO/CdS, ZnO/CdSe, and ZnO/CdS/CdSe photoanodes under visible light illumination (>420 nm) with the applied bias of 0.5 V versus SCE.

visible-light illumination in a potential range of −1.4 to 1.2 V versus SCE, and the scan rate is 10 mV/s. It can be clearly seen that all sensitized photoanodes exhibit enhanced photoresponse current density compared to that of the pristine ZnO, which originates from the expanded absorption range of CdS and CdSe over the visible light. At 1.2 V, the photocurrent of single-shelled ZnO/CdS and ZnO/CdSe NRAs is 16.02 and 10.20 mA/cm^2, respectively, which acquires an increase of 36.4 and 23.2 times compared to the value for ZnO NRAs (0.44 mA/cm^2). In comparison to the single-shelled photoanode, the double-shelled ZnO/CdS/CdSe NTAs photoanode exhibits a much higher current density at the same potential and shows the maximum photocurrent density of 20.03 mA/cm^2. The corresponding photocurrent density responses to repeated light on−off cycles are also presented in Figure 5b; the photocurrent density appears instantly and increases sharply under visible-light illumination but reduces to zero promptly as soon as the illumination is stopped. As expected, the photocurrent density responds following the order of ZnO/CdS/CdSe porous NTAs > ZnO/CdS NRAs > ZnO/CdSe NRAs > ZnO NRAs, which also demonstrates a remarkable improvement in the visible-light absorption and suppression of charge recombination of ZnO/CdS/CdSe porous NTAs. Moreover, the photocurrent density stability test of the as-prepared samples was performed under visible light illumination for 1 h with the applied bias of 0.5 V. As displayed in Figure S6 in the Supporting Information, the photocurrent density with time is quite stable for ZnO/CdS/CdSe porous NTAs, about 89.37% is remained at the end of illumination, suggesting the high stability in the photoelectrochemical application.

To further understand the underlying mechanism for electrical conduction properties in the as-prepared photoanodes, we collected Mott−Schottky (M−S) plots. On the basis of the Schottky barrier between the electrolytes and semiconductor materials, M−S measurement was performed to determine the carrier density.[40] Figure 6 shows the M−S plots

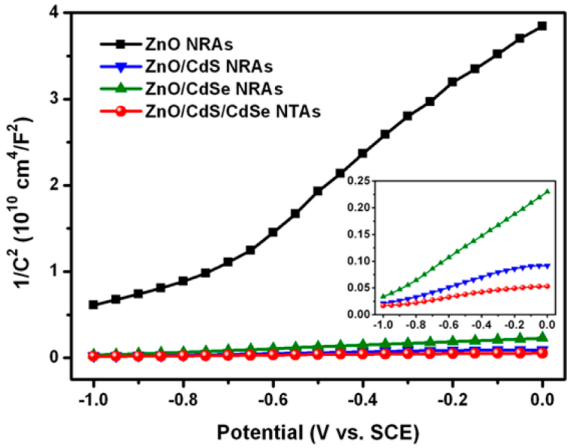

Figure 6. Mott−Schottky plots of the ZnO, ZnO/CdS, ZnO/CdSe, and ZnO/CdS/CdSe measured at a frequency of 10 kHz with an AC imposed bias of 5 mV in 0.25 M Na_2S and 0.35 M Na_2SO_3 electrolyte in the dark.

generated from the capacitance values. It can be observed that all the single and double-shelled photoanodes exhibit much smaller positive slopes than did pristine ZnO, indicating that more donor density appeared after the deposition of CdS and CdSe. Furthermore, the carrier density of the samples can be estimated according to the following equation:[41]

$$N_d = (2/\varepsilon\varepsilon_0 e_0)[d(1/C^2)/dV]^{-1} \quad (1)$$

where ε is the material's dielectric constant, ε_0 is the permittivity of the vacuum, e_0 is the electron charge, V is the potential applied at the electrode, and N_d is the dopant density. With the ε value of 10 for ZnO, CdS, and CdSe and the ε_0 value of 8.85×10^{-12} F m^{-1} for the permittivity of the vacuum, the electron density values are calculated to be 7.87×10^{19}, 3.48×10^{21}, 1.38×10^{21}, and 6.81×10^{21} of ZnO, ZnO/CdS, ZnO/CdSe, and ZnO/CdS/CdSe, respectively. Apparently, the carrier density of the photoanodes also complies with the orders in photoelectrochemical measurement. The ZnO/CdS/CdSe porous NTAs display the highest carrier density and increase about 86.5 times compared to the values for pristine ZnO NRAs; the change can be mainly attributed to the cosensitization effect and porous nanotube, which provides more efficient separation and a longer lifetime for the photoinduced electron−hole pairs.

The photoelectrocatalytic (PEC), photocatalytic (PC), and electrocatalytic (EC) degradation of MB solution were conducted on the as-prepared photoanodes under visible light illumination with an anodic bias of 0.5 V versus SCE. As shown in Figure 7a, the MB molecule is stable under light illumination, and the photolysis efficiency of MB solution can be ignored.

DOI: 10.1021/acsami.5b03527
ACS Appl. Mater. Interfaces 2015, 7, 16387−16394

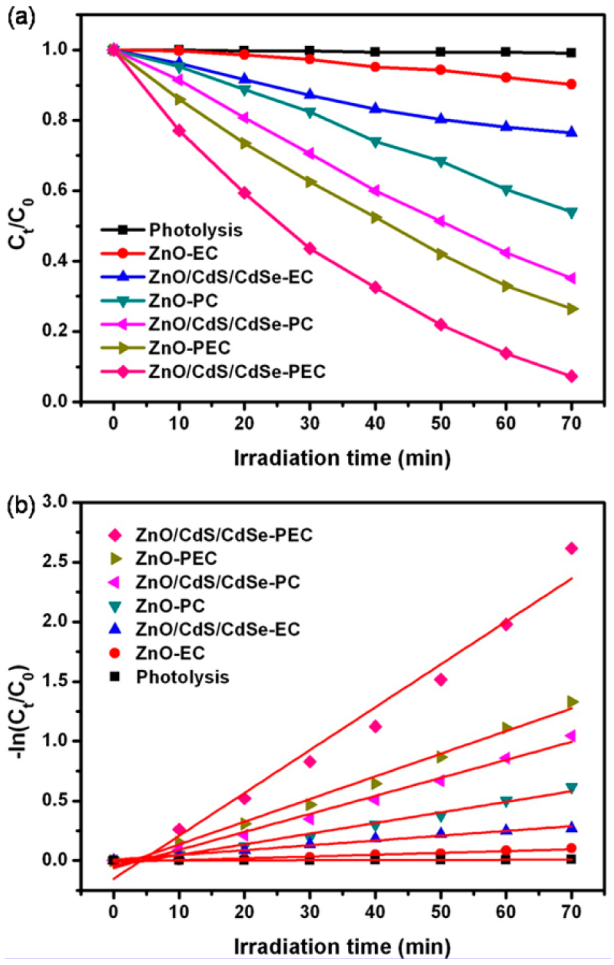

Figure 7. (a) EC, PC, and PEC degradation rates of MB solution on bare ZnO NRAs and ZnO/CdS/CdSe porous NTAs photoanodes. (b) The corresponding plots of $-\ln(C_t/C_0)$ versus irradiation time.

Compared with pristine ZnO NRAs, the PEC, PC, and EC efficiencies of the ZnO/CdS/CdSe porous NTAs are significantly improved; 92.68% of the MB removal rate was achieved after 70 min of the PEC process, while only 64.84% and 23.58% were removed by PC and EC processes during the same irradiation time. The results demonstrate that there may be an apparent synergetic effect between the PC and EC process. Figure 7b presents the kinetic behaviors of MB degradation on the ZnO NRAs and ZnO/CdS/CdSe NTAs; the degradation rates of the MB solution follow the pseudo-first-order reaction according to the simplified Langmuir–Hinshelwood model, $-\ln(C_t/C_0) = kt$, where C_0 is the initial concentration of MB solution, C_t is the concentration of that at different intervals during the degradation process, and k is the reaction rate constant (min^{-1}). The rate constants of all ZnO/CdS/CdSe porous NTAs are significantly higher than that of pristine ZnO NRAs. Furthermore, the ZnO/CdS/CdSe porous NTAs obtain the highest PEC rate constant (0.0359 min^{-1}). Additionally, the PEC, PC, and EC processes of ZnO/CdS and ZnO/CdSe NRAs were also performed to make a comparison, as shown in Figure S7 in the Supporting Information. Figure 8 exhibits the degradation rates of different photoanodes; it can be observed that the degradation efficiency of each catalysis type for ZnO/CdS and ZnO/CdSe NRAs lie between those of the ZnO NRAs and ZnO/CdS/CdSe porous NTAs. Moreover, the catalytic activity of the double-shelled photoanode is

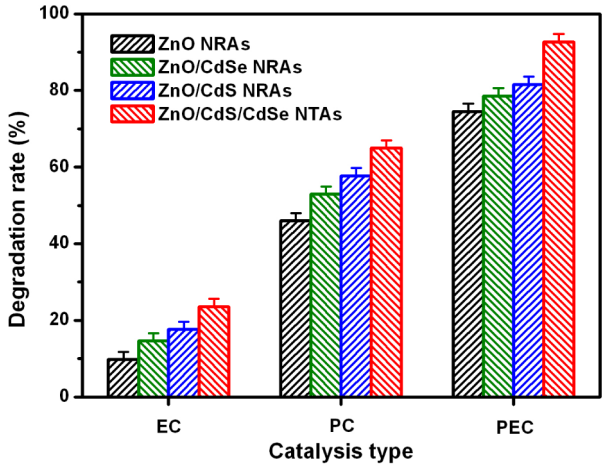

Figure 8. Degradation rates for MB solution by different catalysis types of the as-prepared photoanodes.

superior to that of the single-shelled photoanode under the same conditions, which highlights that the coexistence of CdS and CdSe as well as porous nanotubes are of great importance for facilitating the separation and transfer of photoinduced electro–hole pairs.

The stability of the ZnO/CdS/CdSe porous NTAs photoanode was conducted by repeating the PEC degradation of MB solution under visible-light illumination. As displayed in Figure 9, the degradation yield remains almost the same after four

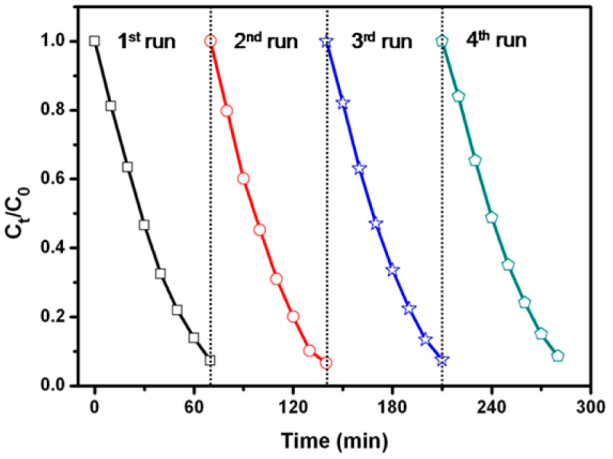

Figure 9. Recycling test of the ZnO/CdS/CdSe porous NTAs photoanode for the PEC degradation of MB solution.

recycled experiments and finally achieves a yield of 91.42%. After deep consideration, the coexistence of CdS and CdSe as well as the nanotube structure may contribute to the favorable photostability, such that the former constructs the type-II mode and separates the charge carries rapidly, and the latter provides a fast transfer channel for electrons that makes the ZnO/CdS/CdSe porous NTA photoanode suffers from few changes in composition and structure. The result suggests that the as-prepared ZnO/CdS/CdSe porous NTAs photoanode exhibits superior photostability and may make a promising candidate for the practical application for organic pollutant degradation under visible light.

In the PEC process of ZnO/CdS/CdSe porous NTAs, the combination of an additional bias voltage and illumination may

DOI: 10.1021/acsami.5b03527
ACS Appl. Mater. Interfaces 2015, 7, 16387–16394

facilitate the photoinduced electron transfer to the counter electrode through the outer circuit and greatly enhance the catalytic activity. As displayed in Figure 10, the cosensitization

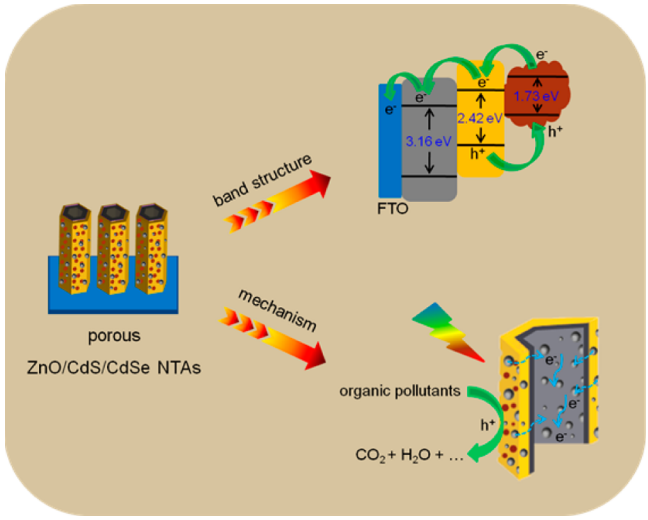

Figure 10. Schematic illustration of the band structure and charge-carrier transfer mechanism for ZnO/CdS/CdSe porous NTAs in the PEC process.

effect and porous nanotube structure provide an efficient pathway for the separation and transfer of the photoinduced electron−hole pairs. After the combination of CdSe and ZnO/CdS, these components are brought into direct and compact contact, and the stepwise band-edge structure is successfully constructed in the type-II mode for ZnO/CdS/CdSe. Under visible-light irradiation, CdS and CdSe can be excited to generate electrons and holes; given that the conduction bands of both CdS and CdSe are more negative than that of ZnO, the energy alignment promotes the photoinduced electrons quickly transferring from CdSe and CdS to ZnO and along the pores in the nanotube to further transport to the FTO substrate and outer circuit. The photoinduced holes transfer and accumulate in the valence band of CdSe to the redox solution, thus exhibiting much higher photocurrent and degradation efficiency than the single-shelled ZnO/CdS and ZnO/CdSe NRAs.

CONCLUSIONS

In summary, we have successfully synthesized a highly efficient double-shelled ZnO/CdS/CdSe porous NTAs photoanode for photoelectrochemical water-splitting and organic pollutant degradation. The as-fabricated ZnO/CdS/CdSe porous NTAs exhibit stronger visible light absorption and more effective separation and transport of photoinduced electron−hole pairs than did single-shelled ZnO/CdS and ZnO/CdSe NRAs, which can be mainly attributed to the following aspects: stepwise band-edge structure, cosensitization effect, and the porous nanotube. The incorporation of merits makes a ZnO/CdS/CdSe porous NTAs photoanode a promising candidate for photoelectrochemical and organic-pollutant-degradation applications.

ASSOCIATED CONTENT

Supporting Information

Figures showing the EDS spectrum of NTAs; SEM and TEM images of NRAs; SAED patterns; EDX spectra of NRAs; XPS spectra; photocurrent density stability test results; and EC, PC, and PEC degradation rates and corresponding plots. The Supporting Information is available free of charge on the ACS Publications website at DOI: 10.1021/acsami.5b03527.

AUTHOR INFORMATION

Corresponding Authors

*Z.-Q.L. E-mail: lzqgzu@gzhu.edu.cn. Tel: 86-20-39366908. Fax: 86-20-39366908.
*J.Z. E-mail: zj2011@whut.edu.cn.

Notes

The authors declare no competing financial interest.

ACKNOWLEDGMENTS

This work was supported by Natural Science Foundations of China (grant nos. 21306030, 21203036, and 51472193), the Guangdong Natural Science Foundation (grant nos. s2013040015229 and 2014A030313520), the Program Foundation of the second batch of innovation teams of the Guangzhou Bureau of Education (grant no. 13C04), the Scientific Research Project of Guangzhou Municipal Colleges and Universities (grant no. 1201410618), and the Fresh Talent Program of Guangzhou University (grant no. 201302).

REFERENCES

(1) Fujishima, A.; Honda, K. Electrochemical Photolysis of Water at a Semiconductor Electrode. *Nature* **1972**, *238*, 37−38.
(2) Sheng, W. J.; Sun, B.; Shi, T. L.; Tan, X. H.; Peng, Z. C.; Liao, G. L. Quantum Dot-Sensitized Hierarchical Micro/Nanowire Architecture for Photoelectrochemical Water Splitting. *ACS Nano* **2014**, *8*, 7163−7169.
(3) Cho, I. S.; Chen, Z. B.; Forman, A. J.; Kim, D. R.; Rao, P. M.; Jaramillo, T. F.; Zheng, X. L. Branched TiO_2 Nanorods for Photoelectrochemical Hydrogen Production. *Nano Lett.* **2011**, *11*, 4978−4984.
(4) Lin, Y. J.; Zhou, S.; Sheehan, S. W.; Wang, D. W. Nanonet-Based Hematite Heteronanostructures for Efficient Solar Water Splitting. *J. Am. Chem. Soc.* **2011**, *133*, 2398−2401.
(5) Yang, P. H.; Xiao, X.; Li, Y. Z.; Ding, Y.; Qiang, P. F.; Tan, X. H.; Mai, W. J.; Lin, Z. Y.; Wu, W. Z.; Li, T. Q.; Jin, H. Y.; Liu, P. Y.; Zhou, J.; Wong, C. P.; Wang, Z. L. Hydrogenated ZnO Core-Shell Nanocables for Flexible Supercapacitors and Self-Powered Systems. *ACS Nano* **2013**, *7*, 2617−2626.
(6) Yu, C. L.; Yang, K.; Xie, Y.; Fan, Q. Z.; Yu, J. C.; Shu, Q.; Wang, C. Y. Novel Hollow Pt-ZnO Nanocomposite Microspheres with Hierarchical Structure and Enhanced Photocatalytic Activity and Stability. *Nanoscale* **2013**, *5*, 2142−2151.
(7) Yang, Y.; Zhang, H. L.; Lin, Z. H.; Liu, Y.; Chen, J.; Lin, Z. Y.; Zhou, Y. S.; Wong, C. P.; Wang, Z. L. A Hybrid Energy Cell for Self-Powered Water Splitting. *Energy Environ. Sci.* **2013**, *6*, 2429−2434.
(8) Schlom, D. G.; Pfeiffer, L. N. Oxide Electronics: Upward Mobility Rocks. *Nat. Mater.* **2010**, *9*, 881−883.
(9) Badre, C.; Pauporte, T. Nanostructured ZnO-Based Surface with Reversible. *Adv. Mater.* **2009**, *21*, 697−701.
(10) Wang, T.; Jin, B. J.; Jiao, Z. B.; Lu, G. X.; Ye, J. H.; Bi, Y. P. Electric Field-Directed Growth and Photoelectrochemical Properties of Cross-Linked Au-ZnO Hetero-Nanowire Arrays. *Chem. Commun.* **2015**, *51*, 2103−2106.
(11) Tong, H.; Ouyang, S. X.; Bi, Y. P.; Umezawa, N.; Oshikiri, M.; Ye, J. H. Nano-Photocatalytic Materials Possibilities and Challenges. *Adv. Mater.* **2012**, *24*, 229−251.
(12) Ahn, K. S.; Yan, Y. F.; Shet, S.; Jones, K.; Deutsch, T.; Turner, J.; Al-Jassim, M. ZnO Nanocoral Structures for Photoelectrochemical Cells. *Appl. Phys. Lett.* **2008**, *93*, 163117.

DOI: 10.1021/acsami.5b03527
ACS Appl. Mater. Interfaces 2015, 7, 16387−16394

(13) Khanchandani, S.; Kundu, S.; Patra, A.; Ganguli, A. K. Shell Thickness Dependent Photocatalytic Properties of ZnO-CdS Core-Shell Nanorods. *J. Phys. Chem. C* **2012**, *116*, 23653−23662.
(14) Xiao, F. X.; Miao, J. W.; Liu, B. Self-Assembly of Aligned Rutile@Anatase TiO_2 Nanorod@CdS Quantum Dots Ternary Core-Shell Heterostructure: Cascade Electron Transfer by Interfacial Design. *Mater. Horiz.* **2014**, *1*, 259−263.
(15) Wang, M.; Jiang, J. G.; Liu, G. J.; Shi, J. W.; Guo, L. J. Controllable Synthesis of Double Layered Tubular CdSe/ZnO Arrays and Their Photoelectrochemical Performance for Hydrogen Production. *Appl. Catal., B* **2013**, *138*−*139*, 304−310.
(16) Xiao, F. X.; Miao, J. W.; Wang, H. Y.; Yang, H. B.; Chen, J. Z.; Liu, B. Electrochemical Construction of Hierarchically Ordered CdSe-sensitized TiO_2 Nanotube Arrays: Towards Versatile Photoelectrochemical Water Splitting and Photoredox Applications. *Nanoscale* **2014**, *6*, 6727−6737.
(17) Liu, Z. Q.; Xie, X. H.; Xu, Q. Z.; Guo, S. H.; Li, N.; Chen, Y. B.; Su, Y. Z. Electrochemical Synthesis of ZnO/CdTe Core-Shell Nanotube Arrays for Enhanced Photoelectrochemical Properties. *Electrochim. Acta* **2013**, *98*, 268−273.
(18) Wang, X. N.; Zhu, H. J.; Xu, Y. M.; Wang, H.; Tao, Y.; Hark, S. K.; Xiao, X. D.; Li, Q. Aligned ZnO/CdTe Core-Shell Nanocable Arrays on Indium Tin Oxide: Synthesis and Photoelectrochemical Properties. *ACS Nano* **2010**, *4*, 3302−3308.
(19) Xu, S.; Wang, Z. L. One-Dimensional ZnO Nanostructures: Solution Growth and Functional Properties. *Nano Res.* **2011**, *4*, 1013−1098.
(20) Wang, X. H.; Koleilat, G. I.; Fischer, A.; Tang, J.; Debnath, R.; Levina, L.; Sargent, E. H. Enhanced Open-Circuit Voltage in Visible Quantum Dot Photovoltaics by Engineering of Carrier-Collecting Electrodes. *ACS Appl. Mater. Interfaces* **2011**, *3*, 3792−3795.
(21) Eley, C.; Li, T.; Liao, F. L.; Fairclough, S. M.; Smith, J. M.; Smith, G.; Tsang, S. C. E. Nanojunction-Mediated Photocatalytic Enhancement in Heterostructured CdS/ZnO, CdSe/ZnO, and CdTe/ZnO Nanocrystals. *Angew. Chem., Int. Ed.* **2014**, *53*, 7838−7842.
(22) Lee, Y. L.; Chi, C. F.; Liau, S. Y. CdS/CdSe Co-Sensitized TiO_2 Photoelectrode for Efficient Hydrogen Generation in a Photoelectrochemical Cell. *Chem. Mater.* **2010**, *22*, 922−927.
(23) Miao, J. W.; Yang, H. B.; Khoo, S. Y.; Liu, B. Electrochemical Fabrication of ZnO/CdSe Core-Shell Nanorod Arrays for Efficient Photoelectrochemical Water Splitting. *Nanoscale* **2013**, *5*, 11118−11124.
(24) Zhang, R.; Luo, Q. P.; Chen, H. Y.; Yu, X. Y.; Kuang, D. B.; Su, C. Y. CdS/CdSe Quantum Dot Shell Decorated Vertical ZnO Nanowire Arrays by Spin-Coating-Based SILAR for Photoelectrochemical Cells and Quantum-Dot-Sensitized Solar Cells. *ChemPhysChem* **2012**, *13*, 1435−1439.
(25) Wang, G. M.; Yang, X. Y.; Qian, F.; Zhang, J. Z.; Li, Y. Double-Sided CdS and CdSe Quantum Dot Co-Sensitized ZnO Nanowire Arrays for Photoelectrochemical Hydrogen Generation. *Nano Lett.* **2010**, *10*, 1088−1092.
(26) Chen, J.; Wu, J.; Lei, W.; Song, J. L.; Deng, W. Q.; Sun, X. W. Co-Sensitized Quantum Dot Solar Cell Based on ZnO Nanowire. *Appl. Surf. Sci.* **2010**, *256*, 7438−7441.
(27) Seol, M.; Kim, H.; Tak, Y.; Yong, K. Novel Nanowire Array Based Highly Efficient Quantum Dot Sensitized Solar Cell. *Chem. Commun.* **2010**, *46*, 5521−5523.
(28) Shen, Y. J.; Lee, Y. L. Assembly of CdS Quantum Dots onto Mesoscopic TiO_2 Films for Quantum Dot-Sensitized Solar Cell Applications. *Nanotechnology* **2008**, *19*, 045602.
(29) Minch, R.; Es-Souni, M. On-Substrate, Self-Standing Hollow-Wall Pt and PtRu-Nanotubes and Their Electrocatalytic Behavior. *Chem. Commun.* **2011**, *47*, 6284−6286.
(30) Qi, X. P.; She, G. W.; Liu, Y. Y.; Mu, L. X.; Shi, W. S. Electrochemical Synthesis of CdS/ZnO Nanotube Arrays with Excellent Photoelectrochemical Properties. *Chem. Commun.* **2012**, *48*, 242−244.
(31) Li, N.; Wang, J. Y.; Liu, Z. Q.; Guo, Y. P.; Wang, D. Y.; Su, Y. Z.; Chen, S. One-Dimensional ZnO/Mn_3O_4 Core/Shell Nanorod and Nanotube Arrays With High Supercapacitive Performance for Electrochemical Energy Storage. *RSC Adv.* **2014**, *4*, 17274−17281.
(32) Su, Y. Z.; Xiao, K.; Liao, Z. J.; Zhong, Y. H.; Li, N.; Chen, Y. B.; Liu, Z. Q. Directed Electrochemical Synthesis of ZnO/PDMcT Core/Shell Nanorod Arrays with Enhanced Photoelectrochemical Properties. *Int. J. Hydrogen Energy* **2013**, *38*, 15019−15026.
(33) Xiao, F. X. Construction of Highly Ordered ZnO-TiO_2 Nanotube Arrays (ZnO/TNTs) Heterostructure for Photocatalytic Application. *ACS Appl. Mater. Interfaces* **2012**, *4*, 7055−7063.
(34) Zhang, J.; Yu, J. G.; Jaroniec, M.; Gong, J. R. Noble Metal-Free Reduced Graphene Oxide-$Zn_xCd_{1-x}S$ Nanocomposite with Enhanced Solar Photocatalytic H_2-Production Performance. *Nano Lett.* **2012**, *12*, 4584−4589.
(35) Xiao, F. X.; Miao, J. W.; Liu, B. Layer-by-Layer Self-Assembly of CdS Quantum Dots/Graphene Nanosheets Hybrid Films for Photoelectrochemical and Photocatalytic Applications. *J. Am. Chem. Soc.* **2014**, *136*, 1559−1569.
(36) Das, S.; Satpati, B.; Chauhan, H.; Deka, S.; Gopinath, C. S.; Bala, T. Preferential Growth of Au on CdSe Quantum Dots Using Langmuir-Blodgett Technique. *RSC Adv.* **2014**, *4*, 64535−64541.
(37) Atuchin, V. V.; Galashov, E. N.; Khyzhun, O. Y.; Kozhukhov, A. S.; Pokrovsky, L. D.; Shlegel, V. N. Structural and Electronic Properties of $ZnWO_4$(010) Cleaved Surface. *Cryst. Growth Des.* **2011**, *11*, 2479−2484.
(38) Li, P.; Zhao, X.; Jia, C. J.; Sun, H. G.; Sun, L. M.; Cheng, X. F.; Liu, L.; Fan, W. L. $ZnWO_4$/BiOI Heterostructures with Highly Efficient Visible Light Photocatalytic Activity: the Case of Interface Lattice and Energy Level Match. *J. Mater. Chem. A* **2013**, *1*, 3421−3429.
(39) Lee, Y. L.; Lo, Y. S. Highly Efficient Quantum-Dot-Sensitized Solar Cell Based on Co-Sensitization of CdS/CdSe. *Adv. Funct. Mater.* **2009**, *19*, 604−609.
(40) Meng, F. K.; Li, J. T.; Cushing, S. K.; Zhi, M. J.; Wu, N. Q. Solar Hydrogen Generation by Nanoscale p-n Junction of p-type Molybdenum Disulfide/n-type Nitrogen-Doped Reduced Graphene Oxide. *J. Am. Chem. Soc.* **2013**, *135*, 10286−10289.
(41) Wu, M.; Chen, W. J.; Shen, Y. H.; Huang, F. Z.; Li, C. H.; Li, S. K. In Situ Growth of Matchlike ZnO/Au Plasmonic Heterostructure for Enhanced Photoelectrochemical Water Splitting. *ACS Appl. Mater. Interfaces* **2014**, *6*, 15052−15060.

DOI: 10.1021/acsami.5b03527
ACS Appl. Mater. Interfaces 2015, 7, 16387−16394